JOURNAL OF THEORETICAL AND APPLIED MECHANICS
45, 4, pp. 833-852, Warsaw 2007

SPACE-TIME/FREQUENCY/SCALE REPRESENTATION OF THE TURBULENCE NEAR THE WALL

F. Sedat Tardu

LEGI BP 53 X 38041 Grenoble Cédex, France
e-mail: sedat.tardu@hmg.inpg.fr

It is proved that the Window Average Gradient (WAG) scheme designed to detect singularities in the turbulence is approximately equivalent to the Hilbert transform of the "Mexican Hat" wavelet. Several identities are derived between these schemes and their validity are theoretically and experimentally shown through the fluctuating wall shear stress and velocity data taken in the turbulent boundary layer. The instantaneous amplitude-frequency representation of WAG at the large scale is also considered. These results indicate that the wall turbulence is significantly regular. It is shown that the near wall singularities involve in the large scale frequency shift key process and that the corresponding instantaneous phase consists of discontinuous line segments.

Key words: near wall turbulence, singularities, wavelet transform, WAG, instantaneous amplitude and phase

1. Introduction

1.1. Aim of the study

Wavelet analysis has become now a classical tool of multirate signal analysis in both time (space) and scale, and found several applications in the analysis of turbulence (Farge, 1992; Akansu and Smith, 1998). One of the major attractive features of this method is its ability of detecting localized singularities independently of the choice of the analysing function. This property makes this tool somewhat universal. Another scheme developed for the same aim, and which will be detailed in Section 1.2, is the Window Average Gradient (WAG) scheme. This paper deals mainly with the interrelationships between these two techniques.

The present study is somewhat inspired by the results presented by De Suza (1997) and De Suza *et al.* (1998). These authors analysed the interaction of a wake generated by a cylinder placed in the inner layer, with the near wall turbulence. They used the Mexican Hat wavelet transform and WAG for pattern recognition of the wake structures. We noticed a remarkable similarity of the conditional pseudo-streamlines, vorticity fields and waveforms resulting from both techniques. Therefore, the first question that arises is whether these methods are identical or not. The answer is not immediate, because of strong (apparent) differences of the analysing functions. We clearly have two targets here: the first one is of practical importance and deals with the clarification of these schemes. The second is of a more general nature and handles the interpretation of the wavelet analysing functions in general.

We aim at giving answers to these questions both theoreticaly and experimentaly in this paper. We first point at the fact that WAG is indeed one of the oldest version of the wavelet analysis, in 1.2.2. We subsequently establish equivalent relationships between the WAG and Mexican Hat wavelet transform by making use of the classical system theory approach. Furthermore, we introduce in Section 2.3 the space (time)-frequency-scale representation of the wavelet transform and, apply it to the singularities detected in the near wall region of a turbulent boundary layer in Section 4.2.

1.2. Background and transfer functions

1.3. Window average gradient scheme

The window average gradient scheme was first introduced by Antonia and Fulachier (1989) and widely used in studies dealing with different flow configurations, for example in Antonia *et al.* (1990), Krogstad and Antonia (1994), De Suza (1997) and De Suza *et al.* (1998). This scheme has been developed to detect discontinuities in fluctuating velocitiy signals and mainly been applied to wall bounded flows, although not exclusively. The continuous version of the WAG detection scheme is defined through a moving window of the width $2T_w$, and the data is transformed into

$$W(t,T_w)=\frac{1}{2T_w}\left(\int_{t}^{t+T_w}u(t)\,dt-\int_{t-T_w}^{t}u(t)\,dt\right) \tag{1.1}$$

where $u(t)$ is the fluctuating turbulent velocity signal. It can be easily seen that $W(t,T_w)$ is the output of a *linear* system whose transfer function $h_W(t)$ is defined by

$$h_W(t) = \begin{cases} \dfrac{1}{2T_w} & \text{for} \quad T_w \leqslant t < 0 \\ -\dfrac{1}{2T_w} & \text{for} \quad 0 \leqslant t < T_w \end{cases} \tag{1.2}$$

and $h_W(t) = 0$ otherwise. Therefore, $W(t, T_w) = u(t) \otimes h_W(t)$, where $\otimes$ stands for the convolution operator. Since the input-output relationships of the linear system are determined through the deterministic autocorrelation function defined as the convolution $\rho w(t) = h_w(t) \otimes h_w^*(-t)$ where the superscript $*$ indicates the complex conjugate. The function $\rho w(t)$ and its energy spectrum $\widehat{\rho} w(\omega) = \widehat{h}_w(\omega)\widehat{h}_w^*(\omega)$ are shown in Fig. 1 and Fig. 2. They will be largely used hereafter.

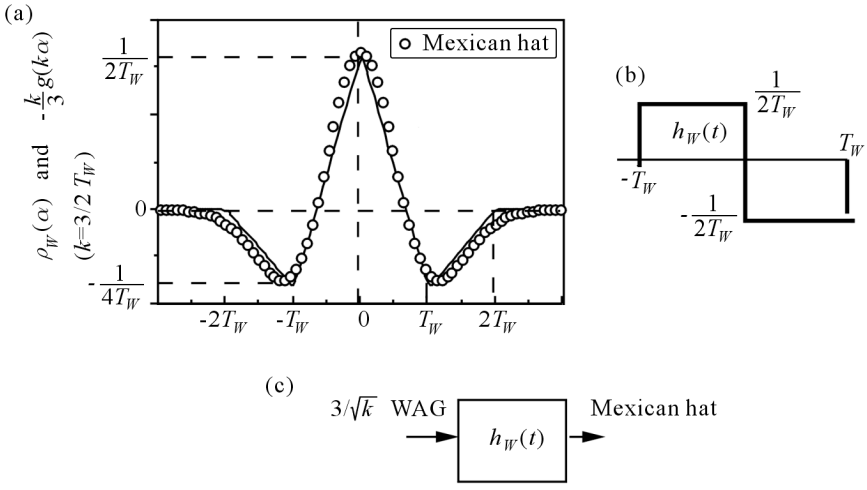

Fig. 1. Correspondance between the window average gradient scheme and the Mexican Hat transform; (a) autocorrelation function of WAG (full line) compared with the modified mother Mexican Hat function (circles); (b) transfer function of WAG, (c) system function between WAG and Mexican Hat

1.3.1. Wavelet transform

The wavelet transform $\Omega(k, t)$ of the signal $u(t)$ is defined by

$$\Omega(k, t) = \sqrt{k} \int_{-\infty}^{\infty} u(\tau) g[k(\tau - t)]\, d\tau = \sqrt{k} u(t) \otimes g(-kt) \tag{1.3}$$

where $g(t)$ is the mother wavelet. The wavelet transform is covariant under time translation and scale change. It conserves the energy of the signal and

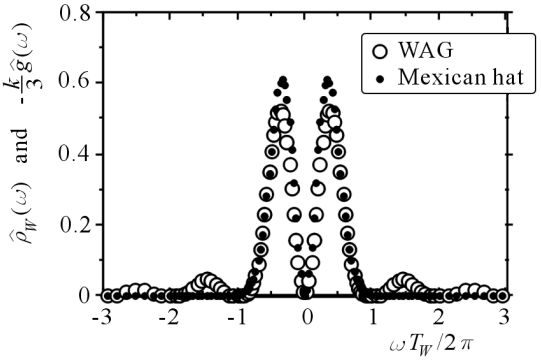

Fig. 2. Fourier transform of the WAG autocorrelation function and of the scaled Mexican Hat mother wavelet

is invertible provided that the admissibility condition is satisfied. The latter implies

$$\int_{-\infty}^{\infty} g(t)\,dt = \int_{-\infty}^{\infty} t^n g(t)\,dt = 0 \tag{1.4}$$

although the second condition of vanishing moments is not compulsory. In the discrete version of the wavelet transform, k and t are often sampled as $k = k_0^m$, $t = nt_0k_0^{-m}$ such that

$$\sqrt{k}g[k(\tau - t)] = \sqrt{k_0^m}g[k_0^m(\tau - nt_0)] = g_{mn}(\tau) \tag{1.5}$$

The coefficients $\Omega(k,t)$ may then be mapped into $\Omega(m,n)$ and the signal is recovered through

$$u(\tau) = \sum_{m=1}^{\infty}\sum_{n=-\infty}^{\infty} \Omega(m,n)g_{mn}(\tau) \tag{1.6}$$

This summation requires an infinite number of terms because of the bandpass character of the wavelet $g_{mn}(\tau)$. In order to express a finite resolution wavelet decomposition at some finite level $m = L$, it is necessary to introduce a complementary low pass *scaling* basis $c_{mn}(\tau)$ in such a way that

$$u(\tau) = \sum_{m=1}^{L}\Big[\sum_{n=-\infty}^{\infty}\Omega(m,n)\frac{1}{2^m}g\Big(\frac{\tau}{2^m} - n\Big) + \sum_{n=-\infty}^{\infty}\Omega(L,n)\frac{1}{2^L}c\Big(\frac{\tau}{2^L} - n\Big)\Big] \tag{1.7}$$

The scaling function $c_{mn}(\tau)$ is generic of what is left in the original signal once the details are sorted out through $\Omega(m,n)$ up to a given scale L. It plays an

important role in the wavelet theory but has not drawn enough attention in the turbulence analysis. Note, for instance, that $c_{mn}(\tau)$ may reveal the characteristics of large scale passive eddies near the wall, when the associated mother wavelet is chosen in some suitable way.

The window averaged gradient scheme defined in (1.1) is per se a wavelet transform since its transfer function $h_w(t)$ is admissible. It is indeed closely related to the Haar transform introduced in 1909 (see for example Meyer, 1992). The later is the simplest wavelet used in multiresolution analysis. Its mother function without translation and dilatation is defined as

$$g_H(t) = \begin{cases} 1 & \text{for} \quad 0 \leqslant t < \frac{1}{2} \\ -1 & \text{for} \quad \frac{1}{2} \leqslant t < 1 \end{cases}$$

and $g_H(t) = 0$, otherwise. It may be easily shown that WAG is a non-causal version of the Haar transform. For a given window time T_W, one has

$$h_W(t - T_W) = \frac{1}{2T_W} g_H\Big(\frac{t}{2T_W}\Big)$$

with the equivalent relationship in the Fourier space

$$\widehat{h}(\omega, T_W) = \mathrm{e}^{j\omega T_W} \widehat{g}_H(2T_W\omega)$$

Furthermore, the complementary scaling functions of WAG and Haar, defined in (1.7), are related through

$$c_W(t - 2T_W) = \frac{1}{2T_W} c_H\Big(\frac{t}{2T_W}\Big)$$

which implies that

$$c_W(t) = \begin{cases} \dfrac{1}{2T_W} & \text{for} \quad -2T_W \leqslant t < 0 \\ 0 & \text{otherwise} \end{cases}$$

The low pass complementary scaling function of WAG corresponds to a time shifted moving average transfer function. The interscale basis coefficients of both schemes are invariant under these transformations. The users of WAG, to the author's knowledge, have not noticed before these equivalences.

One may imagine and construct an infinite number of admissible mother wavelets depending upon the type of multiscale analysis one wishes to perform.

One of the most widely used real wavelets in studies dealing with turbulence is the Marr wavelet (called also the "Mexican Hat") which is the second derivative of Gaussian with the analysing function given by

$$g(t) = (t^2 - 1)\exp\Big(-\frac{t^2}{2}\Big) \tag{1.8}$$

The reason of popularity of this transform may be explained by its efficiency in detecting the discontinuities. The Marr transform is indeed equivalent to the smoothing of the signal by a Gaussian and to its subsequent Laplacian. It focuses, therefore, on the edges of sharp temporal variations. For more details concerning the wavelet transform, we refer to an extensive bibliography provided in a recent book edited by Akansu and Smith (1998).

2. Comparison between the window average gradient scheme and the wavelet transform by Mexican Hat

2.1. Direct correspondence between the autocorrelation function of WAG and the transfer function of "Mexican Hat"

There is a curious coincidence between the detection scheme of WAG and the "Mexican Hat" abbreviated as MH hereafter. Figure 1a shows that the correlation function $\rho_W(\alpha)$ of WAG is well approximated by

$$\rho_W(\alpha) \approx \frac{k}{3}(1 - k^2\alpha^2)\exp\Big(-\frac{k^2\alpha^2}{2}\Big) = -\frac{k}{3}g(k\alpha) \tag{2.1}$$

when the scale dilatation parameter is set as $k = 3/(2T_W)$. It is recalled that g stands for the convolution operator occurring in the Mexican Hat. The fact that the kernel of MH compares well with the deterministic correlation function of WAG via a scaling factor, may also be checked by comparing their respective Fourier transforms

$$\widehat{\rho}_W(\omega) = \frac{4}{\omega^2 T_W^2}\sin^4\frac{\omega T_W}{2} \tag{2.2}$$

and

$$-\frac{k}{3}\widehat{g}(\omega) = \frac{4\sqrt{2\pi}}{27}\omega^2 T_W^2\exp\Big(-\frac{2\omega^2 T_W^2}{9}\Big) \tag{2.3}$$

where $k = 3/(2T_W)$ has been used to obtain the last relationship. Figure 2 shows these distributions versus $\omega T_W/(2\pi)$. The correspondence between

$\widehat{\rho}_W(\omega)$ and $-k\widehat{g}(\omega)/3$ is quite satisfactory despite some differences, in particular near the local maxima where $-k\widehat{g}(\omega)/3$ is slightly larger. The damped small oscillations at high frequencies inherent in $\widehat{\rho}_W(\omega)$ are absent in $-k\widehat{g}(\omega)/3$ but their effect are presumably negligible. Notice furthermore that the deterministic autocorrelation function $\rho_W(\alpha)$ of WAG is admissible in terms of wavelet terminology, i.e it has zero mean, since $\widehat{\rho}_W(0) = 0$.

These observations lead us to conclude that the correlation function of WAG is a satisfactorily linearized version of the function $-kg(k\alpha)/3$. Consequently, one may easily relate the MH transform of a stochastic signal $u(t)$ to its WAG transform. The MH transform $\Omega(k,t)$ of $u(t)$ is indeed nearly equal to

$$\Omega(k,t) = \sqrt{k}u(t) \otimes g(-kt) \approx -\frac{3}{\sqrt{k}}u(t) \otimes \rho_W(t) \tag{2.4}$$

One has therefore

$$\Omega(k,t) \approx -\frac{3}{\sqrt{k}}u(t) \otimes [h_W(t) \otimes h_W^*(-t)] \tag{2.5}$$

and finally

$$\Omega(k,t) \approx \frac{3}{\sqrt{k}}W\Big(t, T_W = \frac{3}{2k}\Big) \otimes h_W(t) \tag{2.6}$$

since $h_W^*(-t) = -h_W(t)$. It is seen that the wavelet transform by "Mexican Hat" is equivalent to the convolution of WAG by its own transfer function, provided that the window averaging time is appropriately chosen. The Mexican Hat transform is clearly a functional defined as the bi-convolution of the stochastic input $u(t)$ by WAG, i.e

$$\Omega(k,t) \approx \frac{3}{\sqrt{k}}W\Big\{W\Big(t, T_W = \frac{3}{2k}\Big)\Big\} = \overline{W}(k,t) \tag{2.7}$$

The function $\overline{W}(k,t)$ is called the WAG induced wavelet and it is abbreviated as WAGIW in the following.

2.2. Indirect correspondence between WAG and Mexican Hat

The wavelet is a bandpass function as one may easily conclude from the admissibilty condition. Furthermore, it has to be *ideal* passband in multiresolution analysis, because the only orthonormal scaling function at full resolution is the ideal *sinc* function which is nothing but the impulse response of an ideal passband filter (Akansu and Smith, 1998; p. 61). The only wavelet satisfying these conditions is the Littlewood-Paley wavelet (Meyer, 1992; p. 26).

In such cases, any spectral decomposition of the form $\widehat{g}(\omega) = \chi(k)\widehat{\rho}(\omega) = \chi(k)\widehat{h}(\omega)\widehat{h}^*(\omega)$ as used in the previous section and where $\chi(k)$ is the scaling factor, leads to a simple conclusion that the amplitude $|\widehat{h}(\omega)|$ is equal to $|\widehat{g}(\omega)|$ via only a modification in the gain, i.e.

$$|\widehat{h}(\omega)| = \sqrt{\frac{|\widehat{\rho}(\omega)|}{\chi(k)}} = \chi'(k)\sqrt{|\widehat{\rho}(\omega)|}$$

Clearly, some but not all the wavelets fulfill these conditions. Yet, one may expect approximation of the latter equality for a given wavelet provided that the spectral decomposition exists. The price to pay for this approximation is ineluctably some leakage of regularity. That is the case for the inter-relationships between the Mexican Hat and WAG transforms and this allows approximation of indirect equivalences between these system functions.

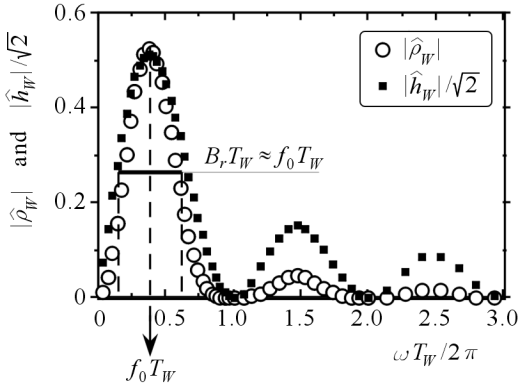

Fig. 3. Amplitude of the Fourier transform of the WAG autocorrelation and transfer functions

Figure 3 compares $|\widehat{h}_W|/\sqrt{2}$ with the amplitude $|\widehat{\rho}_W|$. The ripples induced by WAG are much more pronounced compared with those observed in $|\widehat{\rho}_W|$ and $|\widehat{\rho}_W| \approx |\widehat{h}_W|/\sqrt{2}$ only approximately. That is nothing but the consequence of poorer frequency localization of the Haar wavelet and of its lack of regularity. Both transfer functions represent approximate bandpass filters with the common central frequency $f_0 \approx 0.36/T_W$ and half-power point bandwith $B_r \approx f_0$. In this sense, $\widehat{\rho}$ is a zero phase shift filter, while WAG is a bandpass quadrature filter with $90°$ phase shift. These filters are therefore not equivalent even though their amplitudes are similar, because their phases differ

significantly. The conversion of $\widehat{h}/\sqrt{2}$ to $\widehat{\rho}$ may be achieved by convoluting the former through Hilbert's transform defined as

$$\widehat{h}_H(\omega) = -j\,\mathrm{sgn}\,(\omega) \begin{cases} -j\omega > 0 \\ j\omega > 0 \end{cases} \tag{2.8}$$

The transfer function related to the Hilbert transform reduces for band-limited turbulent signals to

$$h_H(\tau) = \begin{cases} \dfrac{1}{2\pi} \displaystyle\int_{-2\pi f_K}^{2\pi f_K} -j\,\mathrm{sgn}\,(\omega) \mathrm{e}^{j\omega\tau}\, d\omega = \dfrac{2}{\pi\tau} \sin^2(\pi f_K \tau) & \text{for} \quad \tau \neq 0 \\ 0 & \text{for} \quad \tau = 0 \end{cases} \tag{2.9}$$

where f_K stands for the Kolmogoroff frequency. These relationships lead to a second equivalence between WAG and Mexican Hat

$$\Omega(k,t) = -\sqrt{3T_W}\breve{W}(t,T_W) \tag{2.10}$$

where $\breve{W}$ denotes the Hilbert transform. Namely, the Hilbert transform of WAG differs from the wavelet transform MH only by the scaling factor equal to $-\sqrt{3T_W}$ (Fig. 4). In other words, MH is nothing but very close to the response of WAG to a quadrature filter. This also shows that, inversely, the Hilbert transform of the wavelet process is related to

$$W(t,T_W) \approx \frac{1}{\sqrt{3T_W}}\breve{\Omega}(k,t) \tag{2.11}$$

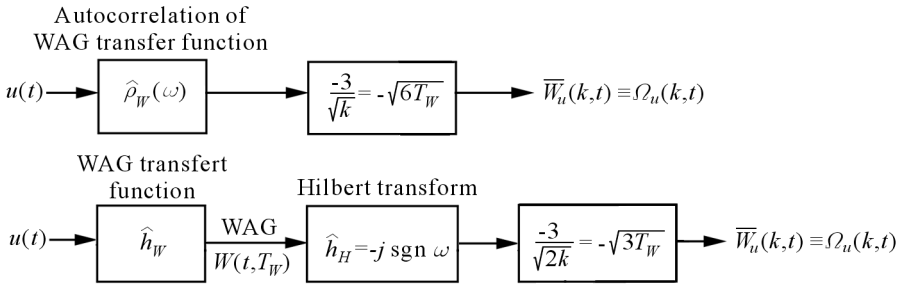

Fig. 4. Hilbert transform of WAG is approximately equivalent to its Mexican Hat transform via a scaling factor

This correspondence is called indirect here, because it appears as a rough estimate compared with the equivalence MH-WAGIW discussed in the previous section. It is however quite satisfactory in some practical situations. It

will indeed be shown in Section 4, through analysis of real signals taken in a turbulent boundary layer, when both sides of (2.10) results in nearly identical traces.

2.3. Rice representation of near wall singularities

The wavelet transform is a bandpass process as we already have recalled. Thus, it lends well itself to the representation as a random modulated signal. The WAG transform, for instance, can be expressed as

$$W(t,T_W) = i(t,T_W)\cos(2\pi f_c t) - q(t,T_W)\sin(2\pi f_c t) \tag{2.12}$$

using Rice's representation (Papoulis, 1984, p. 318; Oppenheim and Schafer, 1975, p. 363). In the last expression, $i(t,T_W)$ and $q(t,T_W)$ are two stochastic processes to be defined and f_c is the carrier frequency. This representation is optimum in the sense of minimizing the average rate of the envelope of $W(t,T_W)$, when the associated dual process equals its Hilbert transform, i.e.

$$\breve{W}(t,T_W) = q(t,T_W)\cos(2\pi f_c t) + i(t,T_W)\sin(2\pi f_c t) \tag{2.13}$$

The optimum carrier frequency is the center of gravity of the WAG spectrum. The inphase component $i(t,T_W)$ and the quadrature component $q(t,T_W)$ are low-pass and their spectrum is constrained into approximately $-f_c/2 < f < f_c/2$. Rewriting equation (2.12) at $t \pm \Delta t$ with $\Delta t = (4f_c)^{-1}$ leads to

$$\begin{aligned} &W(t+\Delta t,T_W) - W(t-\Delta t,T_W) = \\ &\quad = -[i(t+\Delta t,T_W) + i(t-\Delta t,T_W)]\sin(2\pi f_c t) + \\ &\quad -[q(t+\Delta t,T_W) + q(t-\Delta t,T_W)]\cos(2\pi f_c t) \end{aligned} \tag{2.14}$$

which, of course, is exact. The processes $i(t,T_W)$ and $q(t,T_W)$ are random. Their prediction at $t+\Delta t$ may be found by mean square estimation (Papoulis, 1984, Ch. 13; Makhoul, 1975). The estimate of $i(t+\Delta t,T_W)$ in terms of $i(t,T_W)$, its first and second time derivatives $i' = \partial i/\partial t$ and $i'' = \partial^2 i/\partial t^2$ is

$$i(t+\Delta t,T_W) = a_1 i(t,T_W) + a_2 i'(t,T_W) + a_3 i''(t,T_W) \tag{2.15}$$

where the notation is not changed but it has to be kept in mind that these are not *exact* but *estimated* values. The coefficients in the last expression are functions of the autocorrelation function $R_{ii}(\tau)$ of $i(t,T_W)$ and of its time

derivatives. By making use of homogeneity and stationarity, one may show that

$$a_1 = \frac{R_{ii}(\Delta t)R_{ii}^{IV}(0) - R_{ii}''(\Delta t)R_{ii}''(0)}{R_{ii}(0)R_{ii}^{IV}(0) - R_{ii}''(0)R_{ii}''(0)} \qquad a_2 = \frac{R_{ii}'(\Delta t)}{R_{ii}'(0)}$$
$$a_3 = \frac{R_{ii}''(\Delta t)R_{ii}(0) - R_{ii}(\Delta t)R_{ii}''(0)}{R_{ii}(0)R_{ii}^{IV}(0) - R_{ii}''(0)R_{ii}''(0)} \tag{2.16}$$

The Taylor series expansion of terms appearing in a_1, leads to

$$a_1 \approx 1 + \frac{\Delta t^4}{6}\frac{R_{ii}^{IV}(0)R_{ii}^{IV}(0) - R_{ii}^{VI}(0)R_{ii}''(0)}{R_{ii}(0)R_{ii}^{IV}(0) - R_{ii}''(0)R_{ii}''(0)}$$

which clearly shows that $a_1 \approx 1$ to the order Δt^4. Following the same procedure, one has

$$i(t - \Delta t, T_W) = a_1 i(t, T_W) - a_2 i'(t, T_W) + a_3 i''(t, T_W)$$

Combining with 2.15 gives:

$$i(t + \Delta t, T_W) + i(t - \Delta t, T_W) = 2\Big[a_1 i(t, T_W) + a_3 \frac{\partial^2 i(t, T_W)}{\partial t^2}\Big] \approx$$
$$\approx 2\Big[i(t, T_W) + a_3 \frac{\partial^2 i(t, T_W)}{\partial t^2}\Big] + O(\Delta t^4)$$

In a similar manner, the mean square estimated prediction of the quadrature component $q(t, T_W)$ results in

$$q(t + \Delta t, T_W) + q(t - \Delta t, T_W) = 2\Big[b_1 q(t, T_W) + b_3 \frac{\partial^2 q(t, T_W)}{\partial t^2}\Big] \approx$$
$$\approx 2\Big[q(t, T_W) + b_3 \frac{\partial^2 q(t, T_W)}{\partial t^2}\Big] + O(\Delta t^4)$$

The coefficients b_1 and b_3 are easily recovered through the autocorrelation function of $q(t, T_W)$ as in (2.16). Expression (2.14) becomes therefore

$$W(t + \Delta t, T_W) - W(t - \Delta t, T_W) \approx -2\breve{W}(t, T_W) + O(\Delta t^2)$$

Combining with (2.10), gives

$$\Omega(k, t) \approx \frac{\sqrt{3T_W}}{2}[W(t + \Delta t, T_W) - W(t - \Delta t, T_W)] + O(\Delta t^2) \approx$$
$$\approx \frac{\sqrt{3T_W}}{2} DW(t, T_W) \tag{2.17}$$

This last relationship is astonishing by its simplicity and may be generalized for any process and its associated Hilbert transform. The right hand side of (2.17) may be interpreted as the centered time derivative of WAG sampled at Δt. Consequently, the Mexican Hat wavelet is simply proportional to the smoothed time derivative of WAG. The same result could be obtained by using simply Taylor series expansion, but the analysis would not be acceptable because of the randomness of the inphase and outphase components. Representation (2.17) is clearly an approximation of the order $O(\Delta t^2)$. It is however a robust estimate because Δt is smaller than the Nyquist sampling period of the inphase and outphase components. Indeed, since the spectrum of *low-pass slowly varying* $i(t, T_W)$ and $q(t, T_W)$ is constrained into $-f_c/2 < f < f_c/2$, the sampling period is $\Delta t_s = 1/f_c$ and $\Delta t = \Delta t_s/4$. It is therefore not astonishing that (2.17) applied to the near wall turbulent time series is quite successful, even when Δt is as large as the outer time scale, as we will show in Section 4.

3. Experiments

The ensemble of measurements reported here have been realized in the low speed wind tunnel of LEGI with a free stream velocity $U_\infty = 4\,\mathrm{m/s}$. The boundary layer and momentum thickness at the test section are respectively $\delta = 34\,\mathrm{mm}$ and $\theta = 3.4\,\mathrm{mm}$. The Reynolds number based on the local momentum thickness is $\mathrm{Re}_\theta = 913$.

Fluctuating wall shear stress and streamwise velocity are analyzed. The wall shear stress measurements are performed by means of a the Cousteix-Houdeville wall Hot-Wire Gauge (HWG) to avoid problems caused by the conduction into the substrate. A wire of $4\,\mu$m diameter is set into a microcavity and flush mounted to the wall. The length of the sensing element is $200\,\mu$m which corresponds to a spanwise extent of $\Delta z^+ = 3$ ($+$ denotes variables scaled by the viscosity and the shear velocity at $X = 1.14\,\mathrm{m}$ from the transition point). Nice results of the statistics of the fluctuating wall shear stress up to 4th moments have been obtained by this probe. The details are available in Tardu (1998).

The sampling frequency is $f_s^+ = 2$. The signals are prefiltered by the Krohn Hite filter at adequate cut off frequencies. The total duration of each record is $T_{tot} = 5000 T_\infty$ where $T_\infty = \delta/U_\infty$ is the outer time scale. This is long enough to ensure the convergence of statistics up to the 4th order moments including those of the time derivative of fluctuating signals. Bucking amplifiers are used to suppress the DC anemometer output at zero velocity, so that the signal

could be amplified before A/D conversion. This conversion is performed with an Analog-Device RTI-800 board (accuracy: 11 bit+sign; 8 channels) installed in a PC. The HWG is calibrated in situ by determining the velocity gradient at the wall with a single hot film probe (TSI 1276-10W, sensing length $\Delta z^+ = 4$). The Hilbert Transform is obtained by using a 64 points digital Finite Impulse Response filter (FIR).

4. Results

4.1. WAG-Mexican Hat equivalence

Figure 5a shows a sample of the instantaneous wall shear stress τ' and its corresponding WAG transform $W_{\tau'}$ versus time. The variables scaled by the inner parameters, i.e. viscosity ν and shear velocity $u_\tau = \sqrt{\tau/\rho}$ are indexed by (+). Therefore, $t^+ = tu_\tau^2/\nu$, $\tau'^+ = \tau'/\tau$, etc. The WAG integration time in Fig. 5a is $T_W^+ = 13$ and that corresponds to half of the outer time scale δ^+/U_∞^+. For the sake of clarity, we opted for a direct presentation of traces instead of using usual contours of the wavelet coefficients in the time-frequency domain.

The intense WAG events are shown by arrows in Fig. 5a. They were identified in a way similar to Antonia and Fulachier (1989) and Krogstad and Antonia, (1994). Thus, an event occurs when $W_{\tau'}^+$ exceeds a given threshold, i.e. $W_{\tau'}^+ \geqslant \pm\beta\sqrt{\tau'\tau'}/\tau$. The sign $\pm$ is selectively used to detect strong transitions in the signal from negative to positive values and vice versa, and they are indicated separately by open and bold arrows in Fig. 5a. The threshold is taken as $\beta = 0.4$. It is clearly seen that WAG detects strong accelerations or decelerations occurring within the given window time and associated with rapid changes of the sign in the signal.

Figure 5b shows the Mexican Hat (MH) and the WAG induced wavelet (WAGIW) transforms of τ' denoted respectively in wall units as $\Omega_{\tau'}^+$ and $\overline{W}_{\tau'}^+$. It is recalled here that the scale dilatation parameter in $\Omega_{\tau'}^+$ is $k^+ = 3/(2T_W^+)$. It is seen in Fig. 5b that the waveforms of MH merge completely into those of WAGIW except for some slight differences occurring from time to time, in particular near the local maxima. A close inspection of different groups of data of total record lengths exceeding several thousand times the outer time scale, revealed that the residual $\Omega_{\tau'}^+ - \overline{W}_{\tau'}^+$ is rarely larger than 15% of $\Omega_{\tau'}^+$. Clearly the wavelet transform through MH and its linearized version WAGIW are equivalent. One may therefore easily interpret the MH transform as strong transitions from negative to positive values of WAG.

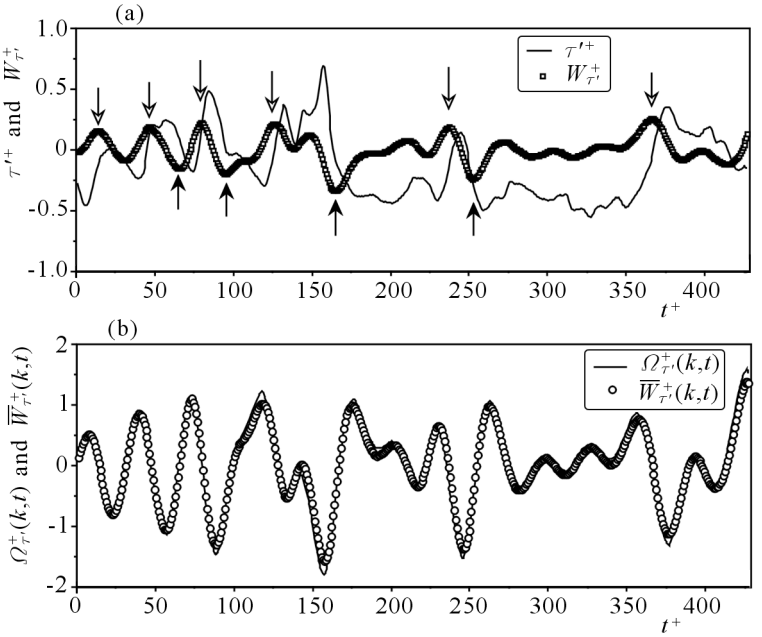

Fig. 5. Sample of instantaneous wall shear stress fluctuations and corresponding wavelet and WAG transforms; (a) instantaneous wall shear stress and its WAG transform in wall units, (b) Mexican Hat transform compared with the WAG induced wavelet transform of the signal shown in (a). The window averaging time and the scale parameter in wall units are respectively $T^+_W = 13$ and $k^+ = 3/(2T^+_W) = 0.11$

This is also confirmed by the analysis of the fluctuating velocity signal $u'(t)$ in the whole boundary layer. Figure 6a shows for instance u'^+ and its WAG transform $W^+_{u'}$ measured in the low buffer layer at $y^+ = 10$ from the wall where the production is nearly maximum. The window average time is now equal to the outer time scale and $T^+_W = \delta^+/U^+_\infty = 26$. It is clearly seen that the coincidence between $\Omega^+_{u'}$ and $\overline{W}^+_{u'}$ is almost perfect (Fig. 6b).

The validity of equation (2.10) relating the Mexican Hat to the Hilbert transform $\breve{W}$ of WAG is now debated through the traces shown in Fig. 7. We only present results concerning the fluctuating wall shear stress as reported in Fig. 5a with $T^+_W = 13$ for the sake of brevity. The main conclusion drawn from Fig. 7 is that there is an excellent agreement between $-\sqrt{3T^+_W}\breve{W}^+_{\tau'}$ and $\Omega^+_{\tau'}$.

We closely inspected, compared and confirmed the validity of equivalences discussed in Section 2, for both the fluctuating wall shear stress and streamwise velocity signals, obtained at different positions $y^+ < 300$ and within a large

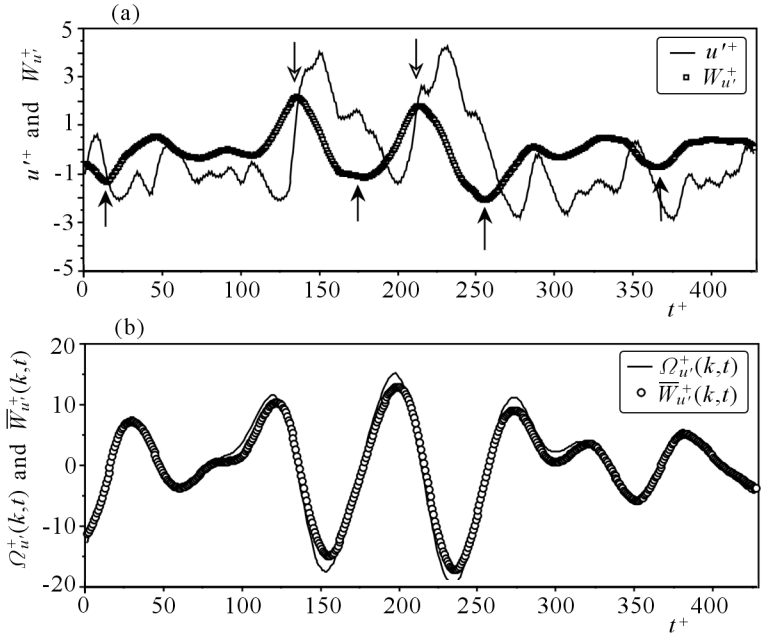

Fig. 6. Sample of instantaneous streamwise velocity fluctuations at $y^+ = 10$ and corresponding wavelet and WAG transforms; (a) instantaneous streamwise velocity and its WAG transform in wall units, (b) Mexican Hat transform compared with the WAG induced wavelet transform of the signal shown in (a). The window averaging time and the scale parameter in wall units are respectively $T_W^+ = 26$ and $k^+ = 3/(2T_W^+) = 0.057$

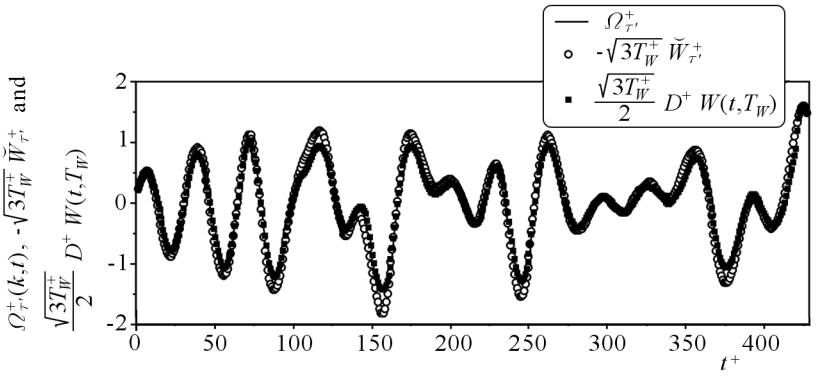

Fig. 7. Comparison of the Mexican Hat transform with the Hilbert transform of WAG and its smoothed time derivative.The raw data is those given in Fig. 5a with $T_W^+ = 13$

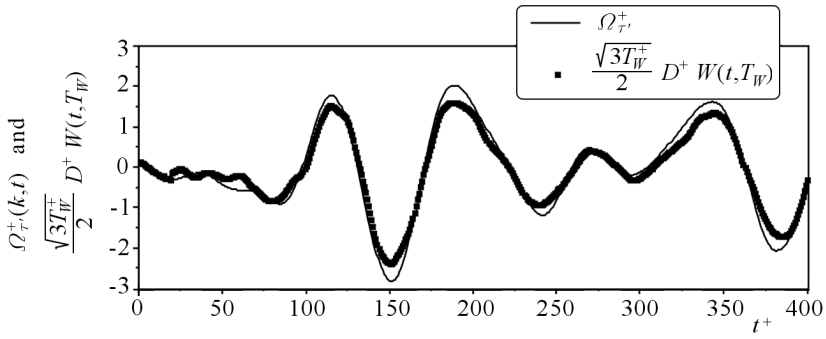

Fig. 8. Comparison of the Mexican Hat transform of the wall shear stress with the smoothed time derivative of WAG given by (2.17) for the largest outer scale integration time $T_W^+ = 26$

range of the window averaging time $3 \leqslant T_W^+ \leqslant 26$. The upper limit in the last expression is the outer time scale, and the inner limit is roughly the Kolmogoroff time scale in the inner layer.

4.2. Time-frequency-scale representation

Any signal, moreover, the wavelet coefficients $\Omega(k,t)$ may be expressed as

$$\Omega(k,t) = r(k,t)\cos\Big[\int_0^t \omega_i(k,t)\Big] \tag{4.1}$$

where $r(k,t)$ stands for the instantaneous amplitude and $\omega_i(k,t)$ is the instantaneous angular frequency at the scale k. This representation is not unique and different characterizations are possible, depending upon the choice of the dual processes. In the Rice canonical representation, that is optimum in the sense of minimizing the average rate of the signal envelope, one has

$$\begin{aligned} r^2(k,t) &= \Omega^2(k,t) + \breve{\Omega}^2(k,t) \\ \omega_i(k,t) &= \frac{\Omega(k,t) \smile \Omega'(k,t) - \Omega'(k,t)\breve{\Omega}(k,t)}{r^2(k,t)} \end{aligned} \tag{4.2}$$

where $(\cdot)'$ denotes the time derivative. The corresponding optimum carrier frequency equals

$$\omega_c(k) = \frac{\overline{r^2(k,t)\omega_i(k,t)}}{\overline{r^2}(k,t)} \tag{4.3}$$

Moreover, the dual of $\Omega(k,t)$ is obviously its Hilbert transform

$$\breve{\Omega}(k,t) = r(k,t)\sin\Big[\int_0^t \omega_i(k,t)\ dt\Big] \tag{4.4}$$

The instantaneous frequency may also be written as

$$\omega_i(k,t) = \omega_c(k) + \frac{d\varphi(k,t)}{dt} \tag{4.5}$$

where $\varphi(k,t)$ is the random phase at the scale k. It is straightforward that $\omega_i(k,t)$ governs directly the behaviour of $\Omega(k,t)$ near the zero-crossings. The transitions from ejections to sweeps detected by the Haar wavelet at large eddy scales behave as the discontinuous phase frequency shift keying process (Papoulis, 1983; Aulin and Sundberg, 1981), with random, yet somewhat coherent and regular periodicity.

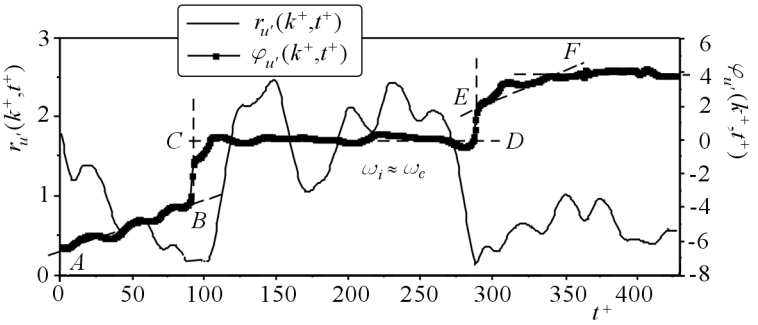

Fig. 9. Samples of the instantaneous amplitude and phase in radians of the Haar wavelet coefficients of the fluctuating streamwise velocity at $y^+ = 10$ versus time. The scale parameter of the wavelet transform is $k^+ = 0.057$ in wall units. CD – constant phase zone wherein the instantaneous frequency is equal to the carrier frequency: singularities are smoothly oscillating due to the meandering of the streaks. AB – the phase increases while the amplitude decreases: apparition of small-scale structures. EF – the phase and amplitude increase simultaneously: active but smaller structures. DE – phase jump

Figure 9 shows some traces of the phase $\varphi(k^+,t^+)$ and amplitude $r^+(k^+,t^+)$ of the fluctuating streamwise velocity signal u' at $y^+ = 10$, for the wavelet scale parameter $k^+ = 0.057$ (corresponding to the wavelet window duration $T_W^+ = 26$). The optimum angular carrier frequency is $\omega_c^+ = 0.08$ in this case. It is seen that the instantaneous phase $\varphi(k,t)$ consists of line segments that are discontinuous at points B and D where random phase jumps occur.

The phase increases first at AB, remains constant during large period CD, jumps again and increases at DF. The constancy of the phase indicates that the instantaneous frequency is sensibly equal to the carrier frequency. The periods like CD wherein $\omega_i \approx \omega_c$ coincide generally with large amplitudes $r^+(k^+, t^+)$. Strong ejection-sweeps transitions marking the arrival of coherent structures are, therefore, merely constant phase events. The time intervals as AB wherein $\varphi(k^+, t^+)$ increases while $r^+(k^+, t^+)$ decreases are reminiscent of apparition of small scales. The slope of AB is $d\varphi^+/dt^+ = \omega_c^+/3$ indicating that $\omega_i(k, t)$ is jumped by a factor 4/3. The jumps in the frequency with the *same* fraction of ω_c^+ are often and repetitively observed. It is asked whether this behaviour can be partly explained by the multifractal nature of the cascade process or not (Argoul *et al.*, 1989). The epochs as EF, wherein both the instantaneous phase and the amplitude increase from small values, are presumably related to the arrival of smaller scale active structures. Note finally that, duration of the segments is about 100-200 wall units that is close to the ejection (bursting) period. The occurrence of these long periods is particularly interesting. These characteristics may eventually be used in the decision loop of some drag-reduction control schemes.

The near wall singularities identified by the Haar wavelet (and for wavelets of any kind such as the classical Mexican Hat) at large integration time may consequently be modeled as the discontinuous frequency shift keying process with random phase discontinuities.

5. Discussion, generalization and conclusion

The relationships deduced in Section 2 were based on the piecewise continuous linearized version of the Mexican Hat mother wavelet. The principal aim was to point at the close similarity between the Haar wavelet designed to detect singularities and the Marr wavelet identifying local maxima or minima. Therefore, the present contribution has to be considered at a first glance, as a "warning" for the users of these schemes. The first of these transforms is the simplest yet the poorest one in terms of frequency localization. The second, on the other hand, stays one of the most popular tools used in the analysis of turbulence data conducted so far. The fact that one may approximately relate both transforms through a simple Hilbert filter and furthermore the smoothed time derivative of the Hilbert transform is quite striking. The analysis leading to this last conclusion, i.e. equation (2.17) is somewhat original and may be generalized for any stochastic process.

On a more general basis, the relationships obtained in Section 2 resulted from the spectral factorization of the linearized Mexican Hat transform. This process can eventualy be generalized at least to the Daubechies's compactly supported wavelets (1992). The transfer function of this family at the Nth iteration may be put in the form of the convolution of N-times WAG with a regularizing polynomial filter. The N-times convolution strengthens the regularity of the wavelet to the order N. The spectral decomposition as conducted here, will then lead to either WAG itself (odd wavelet) or its Hilbert transform (even wavelet) via a scaling parameter. Lewalle (1994) has pointed out that "the exploration of options reveals a large (and rapidly growing) number of wavelets, possibly giving the reader the impression that wavelet selection is arbitrary and the ensuing results biased". We clearly claim out here that the simplest WAG (Haar) wavelet and its Hilbert transform, despite their bad frequency localizations, seem to be adequate enough to characterize the (sufficiently regular) near wall turbulence in the inner region, and more information can hardly be extracted by refining or redefining any other one directional multiscale wavelet which, after all, can always be linked to WAG in some way.

References

1. Akansu A.N., Smith M.J.-T., 1998, *Subband and Wavelet transforms; Design and Applications*, Kluwer Academic Publishers; Boston/Dordrecht/London; Second Printing
2. Antonia R.A., Bisset D.K., Browne L.W.B., 1990, Effect of Reynolds number on the organized motion in a turbulent boundary layer, *J. Fluid Mech.*, **213**, 267-286
3. Antonia R.A., Fulachier L., 1989, Topology of a turbulent boundary layer with and without wall suction, *J. Fluid Mech.*, **198**, 429-451
4. Aulin T., Sundberg C.E.-W., 1981, Continuous phase modulation, *IEEE Trans. Commun., COM-29*
5. Daubechies I., 1992, *Ten Lectures on Wavelets*, SIAM, Philadelphia, PA.
6. De Suza F., 1997, *Etude expérimentale de l'intéraction sillage/paroi dans une couche limite turbulente manipulée*, PhD Thesis, Université de Poitiers, France
7. De Suza F., Delville J., Lewalle J., Bonnet J.-P., 1998, On the large scale organization of a turbulent boundary layer disturbed by a circular cylinder, *Proceedings of 11th Symp. on Turbulent Shear Flows*, 33-25, Grenoble, France

8. Farge M., 1992, Wavelet transforms and their applications to turbulence, *Annu. Rev. Fluid Mech.*, **24**, 395-457

9. Krogstad P.-A., Antonia R.A., 1994, Structure of turbulent boundary layers on smooth and rough walls, *J. Fluid Mech.*, **277**, 1-23

10. Lewalle J., 1994, Wavelet analysis of experimental data: some methods and the underlying physics, *AIAA Paper*, **94-2281**

11. Makhoul J., 1975, Linear prediction: a tutorial review, *Proc. of the IEEE*, **63**

12. Meyer Y., 1992, *Les ondelettes; Algorithmes et applications*, Armand Colin, Paris

13. Oppenheim A.-V., Schafer R.-W., 1975, *Digital Signal Processing*, Prentice-Hall Inc., New Jersey

14. Papoulis A., 1982, Random modulation: a review, *IEEE Transactions on Acoustics, Speech and Signal Processing*, **ASSP-31**, 1, 96-105

15. Papoulis A., 1984, *Probability, Random Variables and Stochastic Processes*, Second Edition; McGraw-Hill, New York

16. Rice S.O., 1945, Mathematical analysis of random noise, *Bell Syst. Tech. J.*, **24**, 46

17. Tardu S., 1998, Near wall turbulence control by time space periodical blowing and suction. Effect of local time periodical blowing, *Exp. Thermal and Fluid Science*, **16**, 1/2, 41-53

Czasoprzestrzenno-częstościowo-skalowy opis turbulencji przyściennej

Streszczenie

W pracy wykazano, że metoda WAG (ang. *Window Average Gradient*) przewidziana do wyszukiwania osobliwości w turbulencji jest w przybliżeniu równoważna transformacji Hilberta falki typu "meksykański kapelusz". Na podstawie badań teoretycznych i doświadczalnych dotyczących fluktuacji naprężeń na ściance oraz rozkładu prędkości w warstwie przyściennej wyprowadzono kilka tożsamości pomiędzy schematami WAG i udowodniono ich prawdziwość. Rozważono także chwilową charakterystykę amplitudowo-częstościową WAG dla dużej skali. Rezultaty analizy wskazały na znaczącą regularność turbulencji przyściennej. Pokazano, że osobliwości obserwowane przy brzegu w dużej skali związane są z procesem przesuwania częstości i odpowiadającym mu nieciągłym zmianom chwilowej fazy.

Manuscript received February 21, 2007; accepted for print April 4, 2007